Attosecond probing of instantaneous ac Stark shifts in helium atoms

2011 J. Phys. B: At. Mol. Opt. Phys. 44 211001

(http://iopscience.iop.org/0953-4075/44/21/211001)

IOP FTC
IOP Publishing
Journal of Physics B: Atomic, Molecular and Optical Physics
J. Phys. B: At. Mol. Opt. Phys. **44** (2011) 211001 (5pp)
doi:10.1088/0953-4075/44/21/211001

FAST TRACK COMMUNICATION

Attosecond probing of instantaneous ac Stark shifts in helium atoms

Feng He[1], Camilo Ruiz[2], Andreas Becker[3] and Uwe Thumm[4]

[1] Key Laboratory for Laser Plasmas (Ministry of Education) and Department of Physics, SJTU, Shanghai 200240, People's Republic of China
[2] Centro de Laseres Pulsados CLPU, Plaza de la Merced s/n E-37008 Salamanca, Spain
[3] Department of Physics and JILA, University of Colorado, Boulder, CO 80309-0440, USA
[4] James R Macdonald Laboratory, Kansas State University, Manhattan, KS 66506, USA

E-mail: fhe@sjtu.edu.cn

Received 18 July 2011, in final form 13 September 2011
Published 19 October 2011
Online at stacks.iop.org/JPhysB/44/211001

Abstract
Based on the numerical solutions of the time-dependent Schrödinger equation within the single-active-electron approximation, we propose a method for observing instantaneous atomic level shifts in an oscillating strong infrared (IR) field with sub-IR-cycle time resolution, by using a single tunable attosecond (SA) pulse to probe excited states of the perturbed atom. The ionization probability in the combined fields depends on both the frequency of the attosecond pulse and the time delay between both pulses, since the IR field periodically shifts SA-pulse-excited energy levels into and out of resonance.

(Some figures in this article are in colour only in the electronic version)

The energetic shift of atomic levels in external electric fields is a well-known phenomenon and usually referred to as 'Stark shift'. For static fields that are much weaker than intra-atomic Coulomb fields, Stark shifts can be calculated using perturbation theory [1]. For oscillating external fields in the optical and near-IR range, perturbation theory breaks down at intensities of about 10^{12} W cm^{-2} [2], orders of magnitudes below the peak intensities available in state-of-the-art ultrashort laser laboratories. If such strong external fields are maintained over many optical cycles, cycle-averaged level shifts can be evaluated, e.g. by exploiting the quasi periodicity of the external field using the non-perturbative Floquet theory [3–5]. However, for the recently developed strong few-cycle IR laser pulses [6–10], atomic level shifts are non-perturbative in nature and also render the continuum-wave Floquet picture inapplicable.

Modern pump-probe experiments combine extended ultraviolet (XUV) attosecond pulses of sub-IR-cycle pulse lengths (1 as $= 10^{-18}$ s) with phase-coherent IR laser pulses to observe electronic dynamics in atoms, molecules and solids [11–16]. The role of laser-dressed highly excited energy levels in atomic excitation and ionization has been studied recently using attosecond technology [17, 18]. In this communication, we show that the attosecond pump-probe technique should also enable the measurement of *instantaneous* level shifts of low-lying bound atomic states in alternating optical electric fields.

To this end, we simulate an XUV pump—IR probe scenario. We choose IR laser fields with negligible distortion of the ground state of He, that are, however, strong enough to couple low excited and continuum states, inducing noticeable level splitting, shift and decay. For the XUV pulses, we fix the number of cycles and vary the central frequency of the pulse. The key to our investigation is the observation that, for a given central frequency ω_{SA} of the single attosecond (SA) pulse and depending on the delay Δt between the pump and the probe pulse, the IR pulse may shift low-lying bound states into or out of resonance with one-photon excitations from the He ground state. The excited atom may then be easily ionized by the IR pulse. If the SA pulse is applied while the instantaneous level energies are off (in) resonance with ω_{SA}, less (more) excitation and thus less (more) ionization out of excited states are expected to occur. This suggests that the detection of the

ionization probability as a function of ω_{SA} and Δt can be used to track the instantaneous Stark shifts.

We will analyse this strategy by modelling He in the so-called single-active-electron approximation (SAEA), in which the time-dependent Schrödinger equation (TDSE) in velocity gauge reads (unless indicated otherwise, we use Hartree atomic units, $e = m = \hbar = 1$)

$$i\frac{\partial\Psi(z,\rho;t)}{\partial t} = \left[\frac{(p_z - A(t)/c)^2 + p_\rho^2}{2} + V(z,\rho)\right]\Psi(z,\rho;t), \quad (1)$$

where z and ρ are the cylindrical electronic coordinates parallel or perpendicular to the laser-polarization axis, respectively, and p_z and p_ρ are the corresponding conjugate momentum operators. $A(t) = c\int_t^\infty \mathrm{d}t' E(t')$ is the vector potential associated with the XUV and IR laser fields and c is the speed of light. The effective potential

$$V(z,\rho) = V(r) = -\frac{1.0 + 1.231\,\mathrm{e}^{-0.662r} - 1.325r\,\mathrm{e}^{-1.236r} - 0.231\,\mathrm{e}^{-0.480r}}{r} \quad (2)$$

with $r = \sqrt{z^2+\rho^2}$ models electronic correlation in terms of screening of the nuclear Coulomb potential by the passive electron [19].

For later reference, we first compute energy-level shifts in the static fields E_{st} in the length gauge. We select a Gaussian initial state $\phi(t=0) = \exp[-(z-2)^2/4 + (\rho-0.2)^2/4]$ that overlaps with the ground and excited states of the Hamiltonian $H_{st} = \frac{p_z^2+p_\rho^2}{2} + V(z,\rho) + zE_{st}$. We then propagate $\phi(t=0)$ numerically and compute the autocorrelation function

$$S(t) = \langle\phi(t=0)|\exp(-\mathrm{i}H_{st}t)|\phi(t=0)\rangle. \quad (3)$$

The real part of the Fourier transformation of the autocorrelation function maps the spectrum of H_{st} in terms of the projected density of states [20, 21]

$$S(E) = \left|\int \mathrm{d}t\, S(t)\exp(-\mathrm{i}Et)\right|^2. \quad (4)$$

We verified that calculations in the velocity gauge give the same numerical results but require smaller time steps than those in the length gauge.

Figure 1 shows the spectrum $S(E)$ for He atoms without external field and in static fields with electric field strengths of $E_{st} = 0.017$, 0.053 and 0.0925. These electric fields E_{st} correspond to laser field intensities of 10^{13}, 10^{14} and 3×10^{14} W cm^{-2}, respectively, for which the ground state of He remains almost unaffected, while the excited 2s and 2p states are shifted to lower and higher energies[5]. For increasing static electric fields, the spectral width of the excited states broadens. We define the level spacings $E^{(static)}_{nl,n'l'}$ as the energy difference between the field-shifted nl and $n'l'$ levels with respect to the position of the maxima in the spectra. The results in figure 1 show that $E^{(static)}_{1s,2s}$ decreases with increasing E_{st}, while $E^{(static)}_{1s,2p}$ increases.

[5] We designate the dressed states by nl, following [4], to indicate their undressed origins.

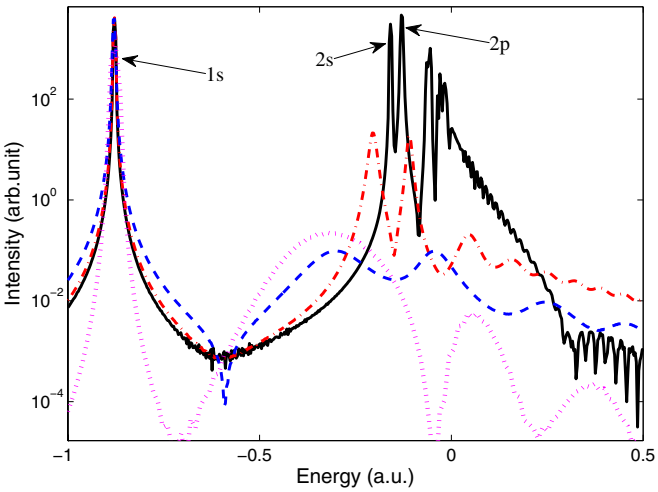

Figure 1. Energy levels for He, calculated in SAEA without (black line) and with static external electric fields corresponding to the laser-field intensities of 10^{13} W cm^{-2} (red dash-dotted line), 10^{14} W cm^{-2} (blue dashed line) and 3×10^{14} W cm^{-2} (magenta dotted line).

Exposed to the combined electric field of a SA pulse and a delayed IR pulse $E_{IR}(t)$,

$$E(t) = E_{SA}\sin(\omega_{SA}t + \phi_{SA})\exp\left[-2\ln 2\left(\frac{t-\Delta t}{\tau_{SA}}\right)^2\right] + E_{IR}\sin(\omega_{IR}t)\cos^2\left(\frac{\pi t}{\tau_{IR}}\right), \quad (5)$$

with $E_{IR} = 0$ if $|t| > \tau_{IR}/2$, level shifts induced by $E_{IR}(t)$ can be probed on an attosecond time scale. ϕ_{SA} is the carrier-envelope phase (CEP) of the SA pulse, which we set equal to zero in all computations, except for the results shown in the right panel of figure 3. We choose Gaussian SA pulses with an intensity of 2×10^{13} W cm^{-2}, a pulse duration τ_{SA} (FWHM) of 2 XUV cycles and variable ω_{SA}, and a $\cos^2$-shaped IR laser pulse with a central wavelength of 800 nm, an intensity of 3×10^{14} W cm^{-2} and a pulse duration τ_{IR} of 4 IR cycles. We neglect the spatial intensity profile of the IR laser pulse since SA pulses can be made to only overlap with the spatial centre of the IR pulse [22, 23].

We determine the ground state of He by imaginary time propagation and use the split-operator Cranck–Nicholson scheme [24] to integrate equation (1) on a numerical grid with equidistant spacings $\Delta z = \Delta\rho = 0.3$ and time steps $\delta t = 0.05$. The spatial grid includes 2000 (400) points and covers the range from -300 to 300 (0 to 120) along the z (ρ) axis. To test the convergence of our numerical results with respect to a further decrease of the spatial and temporal mesh sizes, we reduced the spacetime grid to $\Delta z = \Delta\rho = 0.2$ and $\delta t = 0.02$. As shown in figure 2 (lower panel), the ionization probabilities obtained for a finer spacetime grid (circles) agree well with those calculated with the coarser grid (dashed line) for the same laser parameters. In particular, the small deviation does not influence the physical interpretation of the results. Thus, we continued to use the first-mentioned set of grid parameters for all subsequent calculations. We also carefully checked that any remaining inaccuracy in the description of

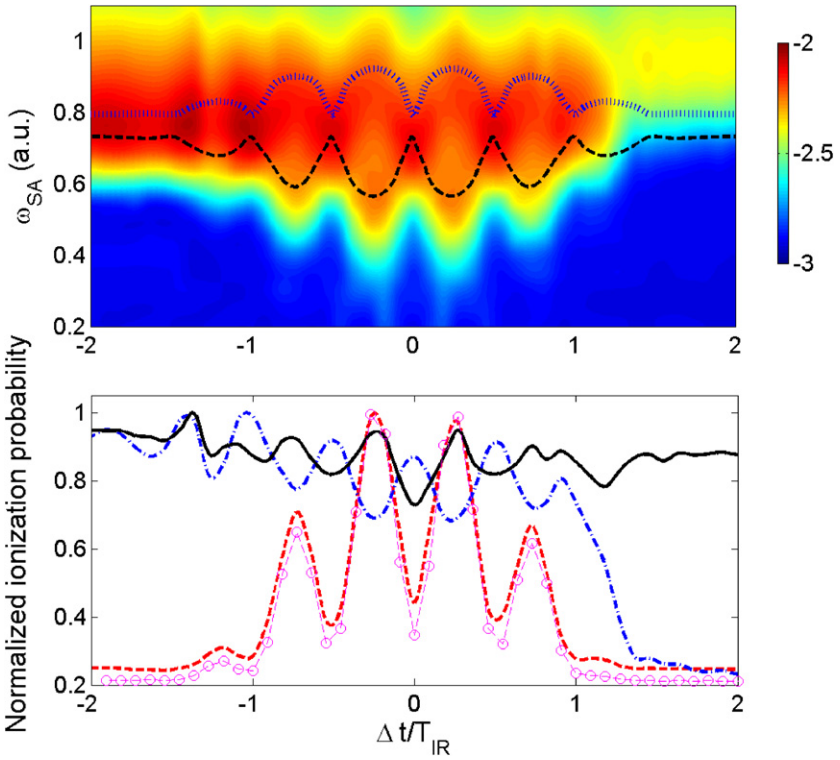

Figure 2. Upper panel: ionization probabilities (logarithmic colour/grey scale) of He calculated in SAEA as a function of the centre frequency $\omega_{\rm SA}$ of the SA pulse and time delay Δt between the SA and IR laser pulses in units of the IR laser period $T_{\rm IR}$. The superimposed dashed and dotted curves show the quasi-static level spacings $E_{1s,2s}^{(\rm static)}$ and $E_{1s,2p}^{(\rm static)}$, respectively. Laser parameters are given in the text. Lower panel: IR-assisted ionization probabilities, normalized to their respective maxima, as a function of Δt for three values of $\omega_{\rm SA}$: 0.5 au (red dashed curve), 0.75 au (blue dash-dotted curve) and 1.1 au (black solid curve). The results represented by the circles are calculated with a finer spacetime grid (see the text) for $\omega_{\rm SA} = 0.5$ au.

the wavefunction at small ρ does not influence the general physical interpretation of the results reported below.

We integrate equation (1) starting at $t = -4\tau_{\rm IR}$ where the vector potential for the IR and XUV fields vanishes. At $t = 4\tau_{\rm IR}$, we continue to propagate the wavefunction until the ionization probability stabilizes. The single-ionization probability is determined as the accumulated outgoing electronic current into the region outside a radius r_0. By varying r_0 between 40 and 60, we confirm that our numerical results for the ionization probability are converged. We use a $\cos^{1/6}$ masking function to suppress reflections from the grid boundaries to a level where the reported ionization probabilities are not affected.

The single-ionization probability P_S is shown in figure 2 (upper panel) on a logarithmic scale. For $\Delta t < 0$, the SA pulse precedes the centre of the IR laser pulse. Accounting for the large bandwidth of the SA pulse, enhanced ionization may occur, even for $\omega_{\rm SA}$ below the ionization threshold, via excitation to an IR laser-dressed bound state followed by ionization in the remaining IR field. Single ionization is thus mediated by either the high-energy side of the XUV-pulse spectrum that extends above the ionization continuum or in a two-step process via transiently excited atoms. Since $P_S(\omega_{\rm SA}, \Delta t)$ behaves differently for different $\omega_{\rm SA}$, we analyse separately three $\omega_{\rm SA}$ intervals. In order to support our interpretations, we present in the lower panel of figure 2 normalized ionization probabilities as functions of Δt, i.e. horizontal cuts through the results presented in figure 2 (upper panel), at $\omega = 0.5$, $\omega = 0.75$ and $\omega = 1.1$.

(1) For $\omega_{\rm SA} < 0.6$, and negligible pulse-overlap ($|\Delta t| > 1.5T_{\rm IR}$, where $T_{\rm IR}$ is the period of the IR field), there is no enhancement of the ionization probability. However, P_S is enhanced and oscillates in the pulse-overlap region ($|\Delta t| < 1.5T_{\rm IR}$) as a function of Δt with period $T_{\rm IR}/2$. P_S reaches maxima when the SA pulse is applied at maximal IR electric-field magnitudes $|E_{\rm IR}|$ (figure 2, lower panel, red dashed line). We explain this behaviour as follows. For $|\Delta t| > 1.5T_{\rm IR}$, the energy gap between the (essentially) field-free 1s and 2p level, $E_{1s,2p}^{(\rm free)} = 0.75$, is larger than $\omega_{\rm SA}$, and the main spectral components of the SA pulse do not overlap with the 2p level. Thus, excitation by the SA pulse is negligible. In contrast, for $|\Delta t| < 1.5T_{\rm IR}$, the dressing by the IR-laser field repeatedly shifts $E_{1s,2s}^{(\rm dressed)}$ into resonance with larger values of $\omega_{\rm SA}$, allowing for efficient excitation followed by ionization in the IR field. The $T_{\rm IR}/2$ oscillation of P_S indicates that $E_{1s,2s}^{(\rm dressed)}$ depends on the *instantaneous* IR intensity which is proportional to $E_{\rm IR}(t)^2$, where $E_{\rm IR}(t)$ is the instantaneous electric field of the IR-laser pulse at time t.

Before proceeding, we note that for our interpretation we have implicitly assumed that the XUV intensities are in the weak-field limit. In order to confirm this assumption,

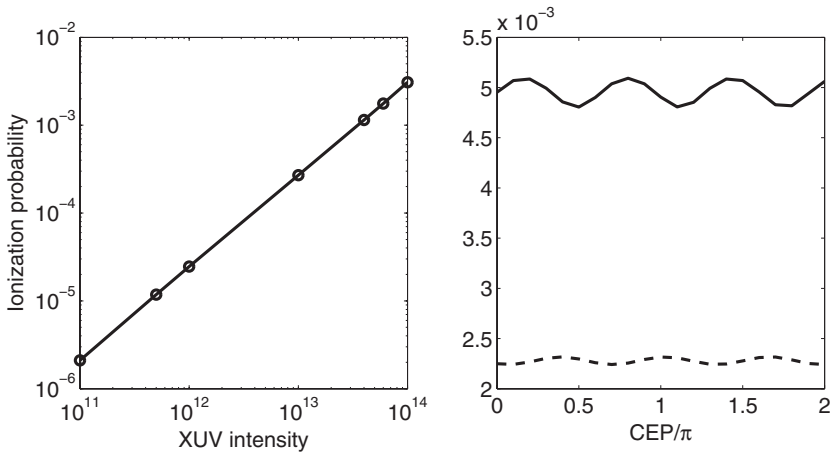

Figure 3. Dependence of the ionization probability on the XUV intensity (left) and the carrier-envelope phase ϕ_{SA} of the SA pulse in units of π (right) for time delays $\Delta t = 0$ (solid line) and $\Delta t = -T_L/4$ (dashed line).

we have computed the ionization probabilities as a function of XUV intensity. Figure 3 (left panel) shows representative results for a time delay $\Delta t = -T_{IR}/4$ and $\omega_{XUV} = 0.5$, which confirm that the ionization probability depends linearly on the XUV intensity in the investigated range of 10^{11}–10^{14} W cm^{-2}. The slope of this solid curve further rules out resonance-enhanced two-XUV-photon ionization as an alternative interpretation of the present results. It also validates that the present interpretation holds at lower XUV intensities, which may be more easily accessible in the experiment.

Furthermore, we investigated the effect of the CEP ϕ_{SA} of the SA pulse on the ionization probability. In figure 3 (right panel), we show the ionization probabilities as a function of ϕ_{SA} at the time delays $\Delta t = 0$ (solid line) and $\Delta t = -T_L/4$ (dashed line). The frequency of the SA pulse is $\omega_{SA} = 0.5$. The fluctuation of the ionization probability for the solid line (dashed line) is less than 2% (3%), which is much smaller than the oscillations in figure 2. We therefore conclude that the CEP of the SA pulse does not affect the modulation of the ionization probability significantly.

(2) If ω_{SA} approximately matches the field-free energy gap $E^{(free)}_{1s,2p}$ and $\Delta t < -1.5T_{IR}$, excitation to the 2p state by the SA pulse followed by subsequent ionization via the IR pulse is very likely. In contrast, the IR pulse by itself is not able to excite and leaves the atom in its ground state. Thus, for $\Delta t > 1.5T_{IR}$, the subsequent not-IR-assisted SA pulse can only excite, but not ionize, the atom. In the overlap region ($|\Delta t| < 1.5T_{IR}$), a small-amplitude IR-laser-induced oscillation of P_S occurs. Maxima in P_S occur at vanishing instantaneous IR intensity (figure 2, lower panel, blue dashed-dotted line), since the energy gap $E^{(dressed)}_{1s,2p}$ increases with field strength which leads to a mismatch with ω_{SA}. In figure 2 (lower panel), the blue dashed-dotted line and red dashed line have opposite carrier phases, since the corresponding energy gaps are asynchronously shifted into and out of resonance with the SA-pulse frequency.

(3) For $\omega_{SA} > 0.8$, the spectrally broad SA pulse may directly ionize He from the ground state, leading to noticeable ionization probabilities even without pulse overlap (figure 2, lower panel, black solid line). The larger ionization probability for $\Delta t < -1.5T_{IR}$ is due to dominant SA-pulse excitation followed by IR ionization, while this two-step mechanism does not apply for $\Delta t > 1.5T_{IR}$. In the overlap region $|\Delta t| < 1.5T_{IR}$, the red dashed and black solid lines are in phase due to synchronous shifts into and out of resonance with $E^{(dressed)}_{1s,2s}$ and $E^{(dressed)}_{1s,2p}$, respectively. Further evidence for the observation of $P_S(\omega_{SA}, \Delta t)$ allowing the detection of instantaneous level shifts is obtained by comparison with the instantaneous quasi-static energy gaps $E^{(static)}_{1s,2s}(t)$ and $E^{(static)}_{1s,2p}(t)$ in the static external field $E_{st} = E_{IR}(t)$, (cf figure 1). The results are drawn as dashed and dotted curves in figure 2 (upper panel) and match the contours of the ionization probability.

For a quantitative investigation, we present the ionization probability P_S in figure 4 as a function of ω_{SA} at three different delays (i.e. as vertical cuts through the results presented in figure 2 (upper panel). At $\Delta t = -T_{IR}/4$ (corresponding to a maximum of $|E_{IR}(t)|$, red dashed line), the instantaneous energy spacings can be identified by the *two* local extrema in P_S. The positions of these maxima as a function of ω_{SA} match the corresponding quasi-static energy gaps $E^{(static)}_{1s,2s}(t)$ and $E^{(static)}_{1s,2p}(t)$ for $E_{st} = |E_{IR}(t)|$ at $t = -T_{IR}/4$. In contrast, application of the SA pulse at a zero of the IR field ($\Delta t = 0$, black solid line) leads to just one maximum in the ionization probability. The position of this maximum as a function of ω_{SA} is slightly shifted to lower frequencies as compared to the field-free energy spacing $E^{(free)}_{1s,2p}$ (blue dash-dotted line for $\Delta t = -2T_{IR}$ in figure 4). This is due to the fact that the SA pulse has a finite non-zero temporal width and probes the (field-dressed) 2s and 2p levels near a zero of the IR field as well.

There is, of course, an intrinsic limitation in the determination of 'instantaneous' energy level shifts. In our proposed method, the observation of the instantaneous energy

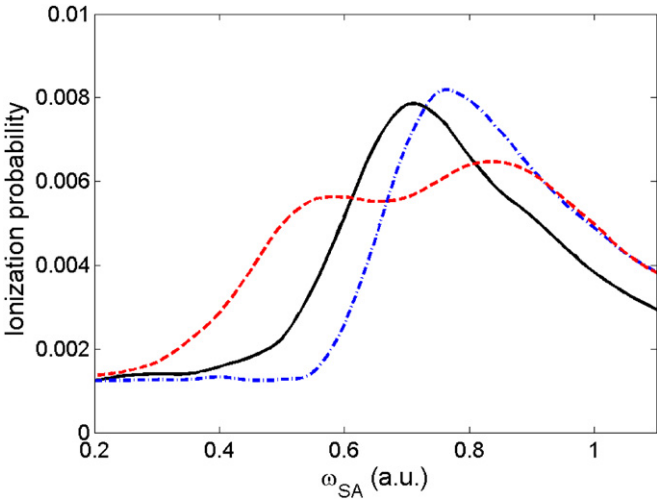

Figure 4. Ionization probabilities as a function of ω_{SA} for three values of $\Delta t/T_{IR}$: -2 (blue dash-dotted line), -0.25 (red dashed line) and 0 (black solid line).

levels is limited by the SA-pulse width. In test calculations, we modified the pulse width of the SA pulse from 2 to 6 optical cycles, and obtained a similar oscillation pattern of the ω_{SA}-dependent single-ionization probability, as shown in figures 2 and 4. For even longer SA pulses, the time-resolved information gets lost, while SA pulses with less than 2 optical cycles blur the results due to their very large spectral widths.

In summary, our simulations indicate that by applying a SA pulse, *instantaneous* energetic shifts in singly excited He induced by a strong few-cycle IR laser pulse are mapped onto oscillations in delay-depended single-ionization probabilities. We interpret these oscillations in terms of a two-step process, where excitation in the SA pulse is followed by efficient ionization out of excited states in the IR field. The excited-state population depends on the instantaneous energy gaps between the ground and excited states in the IR-laser field. Knowledge of the instantaneous energy levels in the strong IR field may lead to new schemes for the coherent control of non-sequential double ionization, high-harmonic generation and molecular dissociation.

Acknowledgments

This work was supported by the Pujiang scholar funding (grant no 11PJ1404800), the NSF of Shanghai (grant no 11ZR1417100) and National Basic Research Program of China (grant no 2007CB310406, 2007CB815105), the new-teacher funding (grant no 201000731200733), the US NSF, the Division of Chemical Sciences, Office of Basic Energy Sciences, Office of Energy Research, US DOE and the MEC FIS 2009-09522 and the Ramón y Cajal Research grants.

References

[1] Bransden B H and Joachain C J 2003 *Physics of Atoms and Molecules* (Singapore: Pearson)
[2] Faisal F H M 1987 *Theory of Multiphoton Processes* (New York: Plenum)
[3] Chu S I and Cooper J 1985 *Phys. Rev.* A **32** 2769
[4] Dörr M, Potvliege R M and Shakeshaft R 1990 *Phys. Rev.* A **41** 558
[5] Rottke H *et al* 1994 *Phys. Rev.* A **49** 4837
[6] Zhou J *et al* 1994 *Opt. Lett.* **19** 1149
[7] Nisoli M *et al* 1997 *Opt. Lett.* **22** 522
[8] Durfee C G, Backus S, Kapteyn H C and Murnane M M 1999 *Opt. Lett.* **24** 697
[9] Apolonski A *et al* 2000 *Phys. Rev. Lett.* **85** 740
[10] Schenkel B *et al* 2003 *Opt. Lett.* **28** 1987
[11] Hentschel M *et al* 2001 *Nature* **414** 509
[12] Itatani J *et al* 2002 *Phys. Rev. Lett.* **88** 173903
[13] Drescher M *et al* 2002 *Nature* **419** 803
[14] Uiberacker M *et al* 2007 *Nature* **446** 627
[15] Cavalieri A *et al* 2007 *Nature* **449** 1029
[16] Goulielmakis E *et al* 2010 *Nature* **466** 739
[17] Johnsson P *et al* 2007 *Phys. Rev. Lett.* **99** 233001
[18] Ranitovic P *et al* 2010 *New J. Phys.* **12** 013008
[19] Tong X M and Lin C D 2005 *J. Phys. B: At. Mol. Opt. Phys.* **38** 2593
[20] Hermann M R and Fleck J A Jr 1988 *Phys. Rev.* A **38** 6000
[21] Chakraborty H and Thumm U 2004 *Phys. Rev.* A **70** 052903
[22] Takahashi E J *et al* 2007 *Phys. Rev. Lett.* **99** 053904
[23] Singh K P *et al* 2010 *Phys. Rev. Lett.* **104** 023001
[24] Feuerstein B and Thumm U 2003 *Phys. Rev.* A **67** 043405